Hypometabolism in Brain of Cognitively Normal Patients with Depressive Symptoms is Accompanied by Atrophy-Related Partial Volume Effects

Matthias Brendel[a], Veronika Reinisch[b], Eva Kalinowski[a], Johannes Levin[c], Andreas Delker[a], Sonja Därr[a], Oliver Pogarell[b], Stefan Förster[d], Peter Bartenstein[a,e], Axel Rominger[a,e,]* for the Alzheimer's Disease Neuroimaging Initiative**

[a]*Department of Nuclear Medicine, University of Munich, Germany;* [b]*Department of Psychiatry, University of Munich, Germany;* [c]*Department of Neurology, University of Munich, Germany;* [d]*Department of Nuclear Medicine, Technical University, Munich, Germany;* [e]*Munich Cluster for Systems Neurology (SyNergy), Munich, Germany*

Axel Rominger

Abstract: Late life depression (LLD) even in subsyndromal stages shows high conversion rates from cognitively normal (CN) to mild cognitive impairment (MCI). Results of [^{18}F]-fluorodesoxyglucose positron-emission-tomography (FDG-PET) were inconsistent in LLD patients, whereas atrophy was repeatedly described. Therefore, we set out to investigate FDG metabolism and the effect of atrophy correction (PVEC) in geriatric CN patients with depressive symptoms. 21 CN subjects with positive item for the depression category (DEP) in the Neuropsychiatric-Inventory-Questionnaire and 29 CN subjects with an absent depression item (NON-DEP) were selected from the ADNI cohort. FDG-PETs were analyzed in individual PET space using volumes-of-interest (VOI) and statistical-parametric-mapping (SPM) approaches. VOI- and MRI-based PVEC were applied to PET data. DEP subjects showed significant hypometabolism in fronto-temporal cortices and the posterior cingulate cortex (PCC) when contrasted against NON-DEP in uncorrected data. Both in VOI- and SPM-based approaches PVEC eliminated significance in PCC, while fronto-temporal regions remained significant or even attained significance such as in case of the left amygdala. Subsyndromally depressed CN subjects had decreased FDG metabolism in mood-related brain regions, which may be relevant to their elevated risk for conversion from CN to MCI. Methodological advances in PET analyses should be considered in future studies as PVEC relevantly changed results of FDG-PET for detecting apparent metabolic differences between DEP and NON-DEP subjects. Furthermore, VOI-based analyses in individual PET space will allow a more accurate consideration of variability in anatomy, especially in subcortical regions.

Keywords: Alzheimer's disease, depressive symptoms, FDG-PET, mild cognitive impairment, MRI, partial volume effect correction.

1. INTRODUCTION

The increasing incidence with age of Alzheimer's disease (AD), the most common form of dementia, is imposing an onerous burden on health care in societies with aging populations [1]. Recent clinical studies have identified associations between late-life depression (LLD) and mild cognitive impairment (MCI) [2], as well as an increased risk for conversion to AD [3]. Indeed, almost one half of AD patients suffer from a depressive syndrome, although the causality is uncertain; the literature is inconclusive whether LLD is a risk factor for AD, or if LLD is rather a prodromal state and early symptom of AD, relevant to the pathophysiology of

AD. Steenland and colleagues noted that factors such as the clinical definition of depression, co-morbidities, age of depression onset, and medication history may be potential confounders in establishing the link between depression and dementia [4]. Brain metabolism, perfusion and anatomy of cognitively normal (CN), mild cognitively impaired (MCI) and demented LLD subjects have been investigated using [^{18}F]-fluorodesoxyglucose positron emission tomography (FDG-PET), H$_2$[^{15}O] PET [5], and magnetic resonance imaging (MRI) [6]. These modalities have suggested some evidence for progressive atrophy and hypometabolism leading to dementia. However, other FDG-PET studies in unmedicated LLD patients have shown inconclusive results with either hypermetabolism [7-11] or hypometabolism [12-15].

Treatment in LLD subjects with antidepressants more consistently led to metabolic decreases in previously hypermetabolic brain areas [16-18]. The metabolic reductions were mainly located in the frontal lobe as well as in the limbic system, i.e. regions involved in executive function and mood, as previously reviewed by Price and Drevets [19]. Indeed, earlier functional studies have particularly implicated medial prefrontal loops within cortico-striato-pallido-

thalamic and amygdalo-striato-pallido-thalamic connections in the pathophysiology of mood disorders [17-19]. The interpretation of observed cerebrometabolic changes in LLD is complicated further by the associations between cerebral atrophy and depression. A longitudinal structural imaging study in MCI subjects has reported progressive atrophy in frontal, parietal and temporal regions [6], while volume reductions in frontal cortex, anterior cingulate cortex (ACC), hippocampus and amygdala were described in CN elderly depressed subjects [20-22], suggesting a causal relationship between atrophy, depression, and conversion to dementia. Recent investigations regarding the link between depression and brain amyloidosis have mainly focused on subjects with remitted earlier depressive episodes and particularly found elevated β-amyloid levels in these patients [23-25]. Regarding this conjecture, an extensive recent longitudinal multi-center study of 8107 CN and MCI subjects showed strong relative risks for the subsyndromally depressed subgroups for conversion either from CN to MCI or from MCI to AD [4]. Here, depression was rated with the Neuropsychiatric Inventory Questionnaire (NPI-Q) or geriatric depression scale (GDS), where NPI-Q served as the stronger predictor for conversion from CN to MCI.

Based on these clinical findings we aimed to utilize the Alzheimer's Disease Neuroimaging Initiative (ADNI) cohort to search for metabolic differences in CN subjects with depressive symptoms (defined by NPI-Q) compared to non-depressed subjects. As cerebral atrophy was presumable in this context [20-22] and influences FDG-PET findings [26] we tested the impact and quantitative influence of partial volume effect correction (PVEC). Furthermore the methodological advance of a volume-of-interest (VOI)-based approach in the individual PET space of each subject was tested with special regard to subcortical regions.

2. MATERIAL AND METHODS

2.1. Alzheimer's Disease Neuroimaging Initiative

Data used in the preparation of this article were obtained from the ADNI database (adni.loni.usc.edu).The ADNI was launched in 2003 by the National Institute on Aging (NIA), the National Institute of Biomedical Imaging and Bioengineering (NIBIB), the Food and Drug Administration (FDA), private pharmaceutical companies and non-profit organizations, as a $60 million, 5-year public-private partnership. The primary goal of ADNI has been to test whether serial MRI, positron emission tomography (PET), other biological markers, and clinical and neuropsychological assessment can be combined to measure the progression of MCI and early AD. Determination of sensitive and specific markers of very early AD progression is intended to aid researchers and clinicians to develop new treatments and monitor their effectiveness, as well as lessen the time and cost of clinical trials.

The Principal Investigator of this initiative is Michael W. Weiner, MD, VA Medical Center and University of California – San Francisco. ADNI is the result of efforts of many co-investigators from a broad range of academic institutions and private corporations, and subjects have been recruited from over 50 sites across the U.S. and Canada. The initial goal of ADNI was to recruit 800 subjects but ADNI has been followed by ADNI-GO and ADNI-2. To date these three

protocols have recruited over 1500 adults, ages 55 to 90,to participate in the research, consisting of cognitively normal older individuals, people with early or late MCI, and people with early AD. The follow up duration of each group is specified in the protocols for ADNI-1, ADNI-2 and ADNI-GO. Subjects originally recruited for ADNI-1 and ADNI-GO had the option to be followed in ADNI-2. For up-to-date information, see www.adni-info.org.

Data from ADNI1, ADNI GO and ADNI2 were included in this work. Pre-processed brain FDG-PET images and corresponding T1-weighted MPRAGE (T1w MRI), matched for time were downloaded from the ADNI database as available on July 30th, 2013.

2.2. Patient Selection and Study Design

As of the cutoff date, the ADNI 1, GO and ADNI 2 databases contained 1338 subjects, of which 398 were clinically rated CN and had undergone brain FDG-PET (Fig. **1**).

Among the CN subjects we defined subjects with depressive symptoms (DEP) and non-depressed (NON-DEP) subjects as subgroups for metabolic comparisons. DEP was defined according to the NPI-Q item #4/12 [27], where existence of any depressive symptoms was binary rated (1 = present; 0 = absent), regardless of the severity [28]. Cases with depressive symptoms did not meet diagnostic criteria for affective disorder, as any subjects meeting criteria for major depression or bipolar disorder had been excluded from ADNI. As other neuropsychiatric symptoms potentially influence brain glucose metabolism as well [29], all subjects reporting symptoms in any of the other eleven domains (e.g. delusions, hallucination, agitation etc.) were excluded from the DEP study group; of 52 DEP subjects, 21 had absence of other neuropsychiatric symptoms.

For the NON-DEP group, a score of zero in the GDS short form [30] was additionally stipulated for inclusion, as NPI-Q and GDS are not strictly correlative [4]. As subjects with intermittent depressive symptoms might likewise have an increased risk of conversion [4], a persistent score of zero in the NPI-Q during a minimum of 24 months follow-up was required for inclusion in the NON-DEP group; among 168 subjects with NPI-Q and GDS of zero at a single visit, 30 fulfilled these criteria during follow-up. Medication status of all included subjects was recorded and checked for psychotropic drugs (antidepressants, antipsychotics, anticonvulsants).

2.3. Image Data

From 30 NON-DEP subjects one was excluded due to cropped cerebellar border in FDG-PET image. Group-wise characteristics of the two study groups are provided in (Table **1**).

A detailed overview of image post-processing and performed analyses is given in Fig. (**2**).

#### *2.3.1. ADNI FDG-PET Acquisition and Pre-Processing*

The FDG-PET images had been acquired using Siemens, GE and Philips PET scanners according to one of three standard protocols (30–60 minute dynamic, 30–60 minute static, 0–60 minute dynamic) following the intravenous injection of
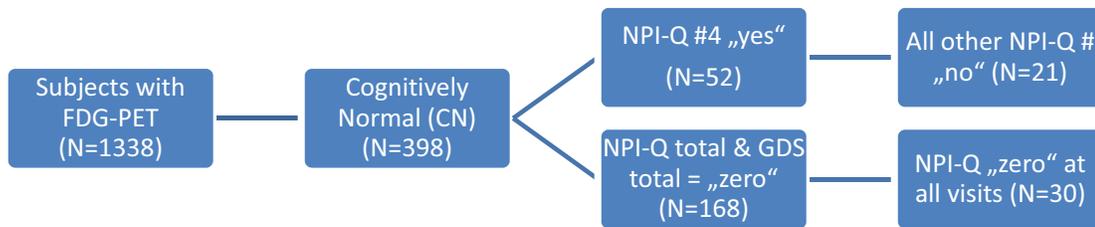
Fig. (1). Subject selection from the whole Alzheimer's Disease Neuroimaging Initiative database. From all available [18F]-fluorodeoxyglucose (FDG) scans, those of cognitively normal patients were selected in the first step. Scores in the Neuropsychiatric Inventory Questionnaire (NPI-Q; 12 items) and the Geriatric Depression Scale (GDS; 15 items) were used to separate subclinical depressed and non-depressed study-groups. # = item-number.

Table 1. Demographics and covariates of the two contrasted study groups, consisting of depressed (DEP) and not depressed (NON-DEP) cognitively normal elderly subjects. MMSE = mini mental state examination. GDS = geriatric depression scale (short form). SD = standard deviation.

	DEP	NON-DEP	p-value
N	21	29	
Age (y), mean ± SD	77.0 +/- 6.9	75.4 +/- 6.3	n.s.
Gender (m/w)	11 / 10	17 / 12	n.s.
Education (y), mean ± SD	16.1 +/- 2.1	15.5 +/- 3.1	n.s.
MMSE (0-30), mean ± SD	29.2 +/- 1.0	29.1 +/- 1.1	n.s.
GDS (0-15)	2.1 +/- 2.1	0	
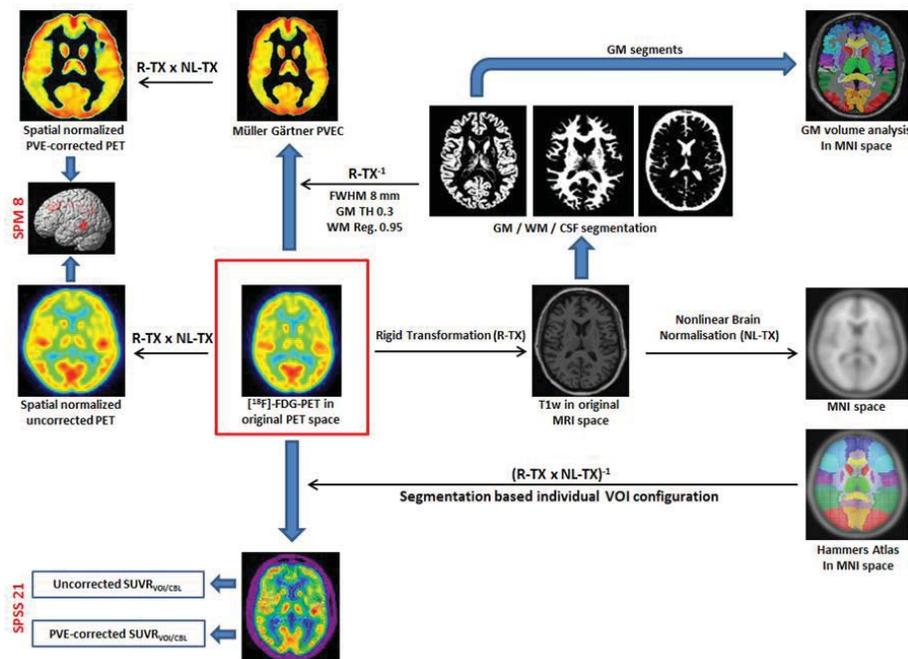
Fig. (2). Processing of [18F]-fluorodeoxyglucose positron-emission-tomography (FDG-PET) and T1-weighted magnetic resonance imaging (T1w MRI) data. Starting from native space PET, rigid (R-TX) and nonlinear (NL-TX) normalizations were performed for spatial matching as required for voxel-wise statistical parametric mapping (SPM). Interpolation was minimized by concatenation of single transformations. T1w MRI images were segmented into gray matter (GM), white matter (WM) and cerebrospinal fluid (CSF) for volume analyses and T1w MRI-based partial volume effect correction (PVEC). Inversion and administration of saved transformations (R-TX^{-1}; NL-TX^{-1}) to the Hammers atlas in Montreal Neurological Institute (MNI) space allowed volume-of-interest (VOI)-based analyses in individual PET space. Resulting uncorrected and PVE-corrected standard-uptake-value-ratios (SUVR) with the cerebellum (CBL) serving as a reference region were analyzed with SPSS. FWHM = full-width-at-half-maximum. GM TH = gray matter threshold. WM reg. = white matter regression.

185 ± 19 MBq of FDG. Data were corrected for both scatter and measured attenuation, which was determined using the CT scan for PET/CT scanners, or a transmission scan with [^{68}Ge] or [^{137}Cs] rotating rod sources for PET-only scanners. Images were reconstructed using scanner-specific algorithms, and sent to the University of Michigan, where they were reviewed for artifacts, anonymized, and transmitted to the Laboratory of NeuroImaging (LONI) for storage. Further details are available in the ADNI PET technical procedures manual (http://www.adni-info.org/Scientists/Pdfs/ ADNI2_PET_Tech_Manual_0142011.pdf).

Downloaded FDG-PET images in DICOM format had been pre-processed in four steps: 1) motion correction by co-registration of single five min frames; 2) time frame averaging (30-60 min p.i.); 3) co-registration of longitudinal data to the baseline scan and reorientation in a standardized 160x160x96 matrix with 1.5 mm cubic voxels; 4) smoothing with a scanner-specific filter function to an isotropic resolution of 8 mm. Details can be found at (http://adni.loni.ucla.edu/methods/pet-analysis/pre-processing/) [31].

2.3.2. ADNI MRI Acquisition and Pre-Processing

T1-weighted MRI scans had been acquired using Siemens, GE or Philips MRI scanners according to a standard protocol [32] involving acquisitions of two 3-D MPRAGE imaging sequences per subject. Of the two images acquired per subject and time-point, the ADNI quality assurance team selected the better image for pre-processing, based on the presence and severity of commonly occurring image artifacts.

MRI preprocessing involved: 1) application of a scanner-specific correction for gradient nonlinearity distortion (Gradwarp) [33]; 2) correction for image intensity non-uniformity (B1) [32]; 3) histogram peak sharpening algorithm for bias field correction (N3) [34]; 4) application of spatial scaling factors obtained by phantom measurements. For images acquired on Philips scanners, B1 correction was already implemented, and the gradient systems with this instrument tended to be linear [35, 36].

2.3.3. Voxel-Wise PET Analyses

2.3.3.1. Co-registration, Smoothing and Normalization

All co-registration procedures were performed using PMOD PNEURO tool (V. 3.407 PMOD technologies). PET images were rigidly co-registered to the corresponding MRI to calculate a linear transformation in MATLAB format (PET-2-MRI). Individual MRI images were nonlinearly co-registered to the standard Montreal Neurological Institute (MNI)-space MRI template, and this transformation was also saved in MATLAB format (MRI-2-MNI). PET-2-MRI and MRI-2-MNI transformations were finally combined and applied to the native space PET images to achieve accurate spatial normalization of PET images with a minimum of interpolation. These images were Gaussian-filtered at 8 mm and intensity-normalized by scaling to the cerebellum VOI [37, 38] defined in the Hammers Atlas [39] for further statistical-parametric-mapping (SPM) analyses (Fig. **2**).

2.3.3.2. MRI-based PVEC

T1-weighted MR images were segmented into gray matter (GM), white matter (WM) and cerebro-spinal fluid (CSF) within original MRI-space using PMOD PNEURO tool [40]. All segmentations were visually checked for correctness and extracerebral artifacts. In cases with such artifacts, we applied binary masking with a whole brain FDG-PET template image in MRI-space. MRI-based PVEC (MGM) [41] was performed in PET space using PMOD with a GM threshold of 0.3, WM regression of 0.95 and full-width-at-half-maximum of 8 mm (= uniform resolution). Resulting PVE-corrected FDG images were saved in PET-space and the MRI-2-MNI transformation was applied. As MGM only accounts for GM-voxels, for further statistical analyses, multiplication of all PET images in MNI-space was performed to generate a mask template for all analyzed subjects including only voxels containing activity > zero. In analogy to uncorrected images, a Gaussian filter of 8 mm and intensity normalization to cerebellum (adapted to the SPM mask) were applied.

2.3.3.3. Voxel-Wise Statistics

Group comparisons of uncorrected and PVE-corrected FDG images were performed voxel-wise using two-sample t-tests in SPM 8 (Wellcome Department of Cognitive Neurology) implemented in MATLAB (R 2011a; MathWorks Inc.). Age, gender, education and mini mental state examinations (MMSE) were used as covariates, with the mask gained from MGM being applied to both analyses in order to make them comparable. DEP and NON-DEP subjects were contrasted using a significance threshold of $p < 0.001$, uncorrected for multiple comparisons and an extent of > 50 voxels; FDG uptake differences were analyzed in both directions separately.
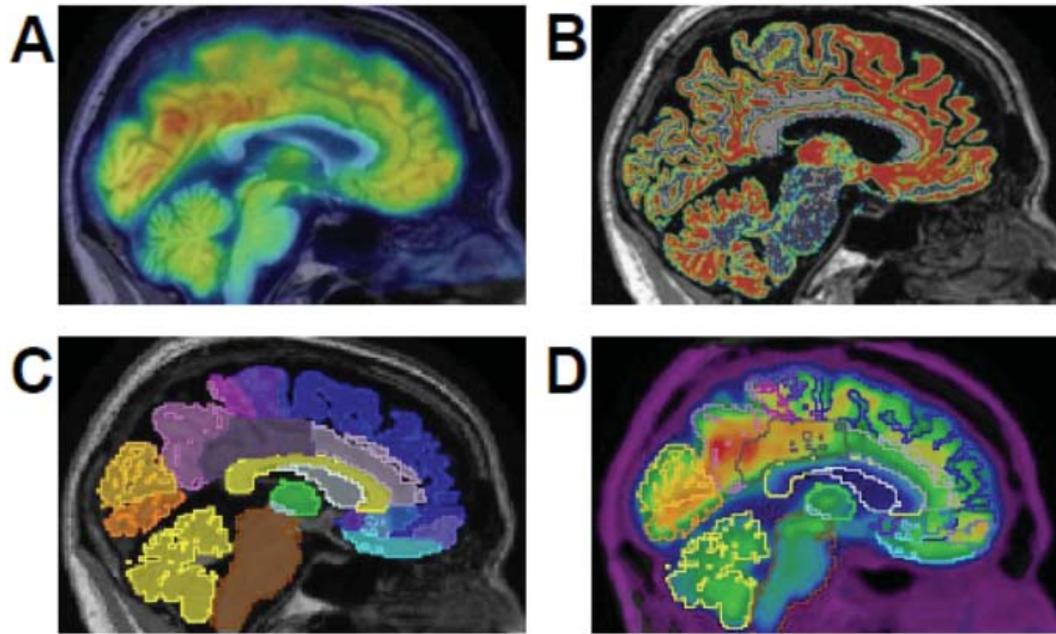
2.3.4. VOI-based PET Analyses

2.3.4.1. Individual VOI Calculation

VOI-based FDG data of all subjects were analyzed in the individual PET-space of all 50 subjects using PNEURO (Fig. **3A-D**).

The algorithm uses individual PET and MRI images as well as a brain segmentation consisting of 83 brain VOIs in the MNI-space, as devised by Hammers [39]. Single subject FDG-PET images were rigidly fused on individual MRIs, which were nonlinearly fused to the MRI-MNI-space template, in analogy to methods described in 2.3.3.1 above. Previously established GM/WM/CSF segmentations were used to generate individual GM-VOIs in the MNI-space segmented in the Hammers atlas. In the next step, the concatenation of the two transformations (PET-2-MRI, MRI-2-MNI) was inverted and applied to the individual VOIs, thus bringing them to the corresponding single subject's native PET-space (Fig. **2**). Additionally, volumes (mm³) of all 83 regions were calculated after transformation of individual VOI templates into the MNI-space.

2.3.4.2. VOI-based PVEC

A VOI-based PVEC [42, 43] was performed with the individual VOIs and both uncorrected and PVE-corrected results were generated. For each non-ventricular VOI, standard-uptake-value-ratios (SUVR) were calculated by dividing the VOI mean value by the cerebellar mean value. Thus, we obtained $SUVR_{VOI/CBL}$ in a total of 75 regions for both uncorrected and PVE-corrected data.

Fig. (3). Representative processing steps for individual volume-of-interest (VOI)-based analyses using PNEURO. First, [^{18}F]-fluorodeoxyglucose positron-emission-tomography (FDG-PET) and T1-weighted magnetic resonance (T1w MRI) images were co-registered by rigid body transformation **(A)**. After gray matter segmentation of the T1w MRI **(B)**, the 83 grey matter volumes-of-interest from Hammers atlas were transformed from Montreal Neurological Institute space to the individual T1w MRI **(C)** and were finally outlined in the individual PET space **(D)** for further analyses including VOI-based partial volume effect correction.
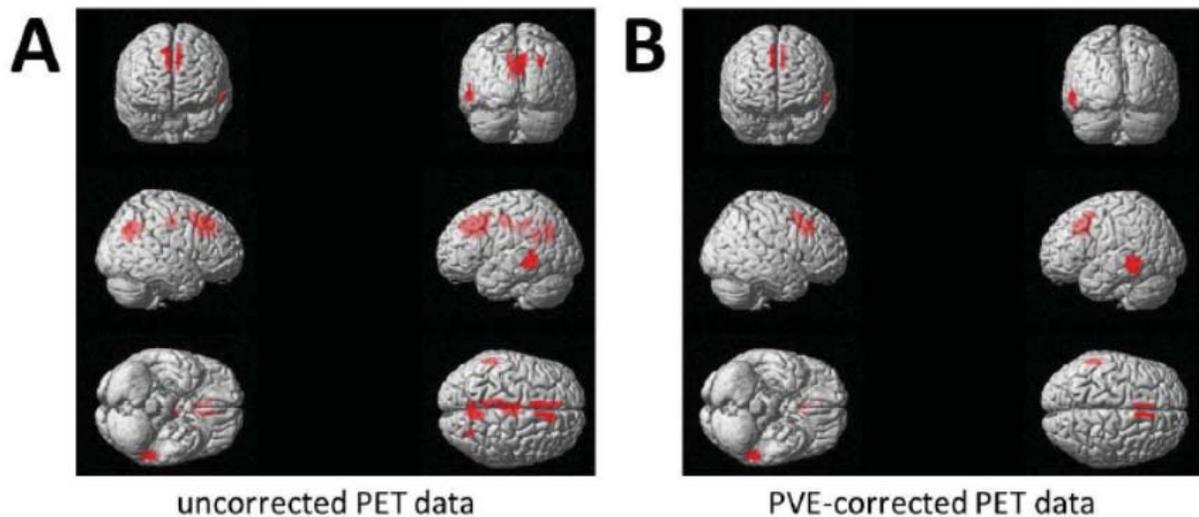
Fig. (4). Results of statistical parametric mapping (SPM) for uncorrected **(A)** and partial volume effect (PVE)-corrected **(B)** contrasts for depressed (N = 21) vs. non-depressed cognitively normal elderly subjects (N = 29). Voxels exceeding a significance threshold of p < 0.001, (unc.; k > 50 voxel) for hypometabolism in depressed subjects are rendered on the standard SPM8 template. No significant voxels were found in the vice versa contrast.

2.3.4.3. Effects of Medication

Uncorrected and PVE-corrected SUVR$_{VOI/CBL}$ results of the DEP subjects were subdivided into medicated (N = 13) – of which nine were treated with serotonin-(noradrenaline)-reuptake-inhibitors (S(N)SRI) – and unmedicated (N = 8) groups to test for possible effects of psychotropic drugs. NON-DEP were drug naive.

2.3.4.4. VOI-based Statistics

Uncorrected and PVE-corrected SUVR$_{VOI/CBL}$ as well as volume values were compared for DEP and NON-DEP subjects with multivariate analysis of covariance (MANCOVA) including age, gender, MMSE and education as covariates using SPSS (version 21.0; SPSS, Chicago, IL). P-values < 0.05 were assigned to be significant.

3. RESULTS

3.1. Demographics

See Table **1** for details of the study population.

3.2. Voxel-wise Analysis

3.2.1. PET Data Uncorrected for PVE

Uncorrected data for DEP subjects showed significant ($p < 0.001$; unc.) unilateral relative hypometabolism in left frontal and temporal cortices together with bilaterally decreased metabolism in anterior and posterior cingulate cortex (ACC/PCC), cuneus, precuneus and paracentral lobule when contrasted against NON-DEP subjects (Fig. **4A,** Table **2A**). There were no metabolic increases even at a more liberal threshold.

3.2.2. PET Data Corrected for PVE

PVE-corrected data of DEP subjects showed a small cluster of significant ($p < 0.001$; unc.) hypometabolism in the left frontal cortical area and additional hypometabolism in right superior frontal gyrus, in the contrast with NON-DEP subjects. Unilateral temporal hypometabolism was similar to that for uncorrected data. Bilateral significant metabolic decreases were still prominent in ACC, but entirely disappeared in the PCC, cuneus and precuneus after PVE correction (Fig. **4B,** Table **2B**). There were no relative metabolic increases.

3.3. VOI-based PET Analysis

3.3.1. Analyses of GM Volumes

Significant differences in GM volumes between DEP and NON-DEP subjects in sense of more atrophy in the DEP group were observed in left PCC (-4.4%; $F = 4.91$; $p < 0.05$), right PCC (-5.8%; $F = 6.48$; $p < 0.05$) and left superior frontal gyrus (-5.6%; $F = 4.56$; $p < 0.05$). Cerebellum volumes were nearly identical between groups (-0.7%; $F = 0.74$; $p = 0.40$).

3.3.2. Uncorrected and PVE-corrected PET Data

Regions with significantly different FDG uptake ($p < 0.05$) between DEP and NON-DEP subjects are reported in Table **3** for uncorrected and PVE-corrected data. Without PVEC, 39 of 75 analyzed regions revealed significantly lower relative metabolism in DEP subjects, mostly pronounced in left and right PCC ($F = 19.0$; $p < 0.001$ / $F = 14.6$; $p < 0.001$) and superior and lateral parietal gyri ($F = 14.3/15.6$; $p < 0.001$). Consistent with SPM results, we also observed hypometabolism in bilateral ACC, frontal, and occipital VOIs, as well as in the left temporal gyri, in absence of PVEC. Additionally DEP subjects showed significant metabolic reductions in deep cortical regions, i.e. the left insular cortex and subcortical structures (thalamus, substantia nigra, nucleus accumbens, putamen and pallidum). Hypometabolism in DEP subjects was hemispherically dysbalanced, with more left hemispheric structures revealing lower FDG uptake (23/39). There were no regional findings of elevated $SUVR_{VOI/CBL}$ in DEP compared to NON-DEP patients.

After VOI-based PVEC, relative hypometabolism was found in only 18 of 75 analyzed regions of DEP subjects.

The bilateral PCC no longer showed a significant reduction after correcting for atrophy ($F = 3.8$; $p =$ n.s.). Formerly significant reductions in bilateral ACC, frontal, parietal and occipital cortices were no longer significant after PVEC, while new significant reductions appeared in the middle temporal gyrus ($F = 5.4$; $p < 0.05$) and the amygdala ($F = 5.0$; $p < 0.05$) after PVEC.

The preponderance of left hemispheric hypometabolism appeared even more prominent after atrophy correction; 15/18 significant different regions were on the left side.

3.3.3. Effects of Medication

13 of 21 DEP subjects received one or more chronic antidepressant, antipsychotic or anticonvulsive medication including SSRI ($N = 8$), SNRI ($N = 3$) or noradrenaline-dopamine-reuptake-inhibitors ($N = 2$), benzodiazepines ($N = 4$), gabapentin ($N = 2$), prinidone ($N = 1$), topiramate ($N = 1$). Subdivision of the DEP group (medicated vs. non-medicated; SSRI vs. non-SSRI) indicated a non-significant trend towards lower metabolism for medicated subjects in bilateral frontal ($F = 2.0$; $p = 0.29$), parietal ($F = 3.4$; $p = 0.21$) and occipital ($F = 1.6$; $p = 0.37$) cortices as well as the left insula ($F = 1.2$; $p = 0.39$) when contrasted against unmedicated subjects. Stable results ($F < 1.0$; $p > 0.5$) in the subgroups were observed in the remaining regions.

4. DISCUSSION

We performed the first FDG-PET comparison of cerebral metabolism analysis in cognitively normal elderly subjects with presence or absence of subsyndromal depressive symptoms. After applying voxel-wise correction for GM-atrophy, hypometabolism remained in the left medial frontal gyrus, bilateral ACC and left middle temporal gyrus in aged DEP subjects. Formerly marked hypometabolism in the posterior cingulate cortex was no longer observed after PVEC and therefore probably atrophy driven. VOI-based $SUVR_{VOI/CBL}$ analyses additionally identified hypometabolism in left insula, left amygdala and bilateral thalami of the DEP group; these areas may furthermore be relevant to the high relative risk for conversion from CN with depressive symptoms to MCI [4].

4.1. Brain Regions Related to Mood Disorders

Our findings of decreased FDG uptake in bilateral thalami, left putamen, left insula, left amygdala and left frontal cortical regions overlap with previously identified mood-related brain networks, and suggest the occurrence of metabolic depression within these same circuits in LLD. Involvement of frontal cortical regions and ACC in mood-disorder related brain networks has been reviewed recently [16]. In particular, mood disorders may involve dysfunction of a medial prefrontal network (including overlapping cortico-striato-pallido-thalamic and amygdalo-striato-pallido-thalamic loops) consisting of parts of the ventromedial surface of the frontal cortex, rostral and ventral to the genu, areas along the medial edge of the orbital cortex, and a small caudolateral orbital region at the rostral end of the insula connects primarily cortico-cortical with the anterior and posterior cingulate cortex [44].

Table 2.   Findings of voxel-wise [18F]-fluorodeoxyglucose (FDG) PET analyses for the contrast between depressed and non-depressed cognitively normal elderly subjects; clusters in data (A) uncorrected for partial volume effects and (B) corrected for partial volume effects. Data indicated in bold font indicate a cluster, and subsequent non-bold data identify sub-peaks within the same cluster. Numeric data are Talairach and Tournoux coordinates transformed from Montreal Neurology Institute space (x, y, z; mm). Cluster extension = number of voxels. R = right. L = left. BA = Brodmann area. uncorr. = uncorrected for multiple comparisons.

2A

Location	Talairach and Tournoux coordinates			peak	p value	cluster
	x	y	z	z-value	uncorr.	extension
L Medial Frontal Gyrus, BA 32	**-5**	**7**	**45**	**4.34**	**< 0.001**	**340**
L Cingulate Gyrus, BA 32	-7	25	39	3.82	< 0.001	
L Superior Frontal Gyrus, BA 8	-9	34	45	3.14	0.001	
R Cingulate Gyrus, BA32	**6**	**21**	**42**	**4.27**	**< 0.001**	**253**
R Precuneus, BA 7	**22**	**-68**	**31**	**4.25**	**< 0.001**	**50**
L Posterior Cingulate, BA 31	**-9**	**-49**	**21**	**4.02**	**< 0.001**	**117**
R Cuneus, BA 7	**6**	**-65**	**32**	**3.92**	**< 0.001**	**477**
R Precuneus, BA 31	2	-68	27	3.84	< 0.001	
R Cuneus, BA 18	4	-73	21	3.25	0.001	
L Paracentral Lobule, BA 31	**-5**	**-19**	**46**	**3.83**	**< 0.001**	**389**
L Cingulate Gyrus, BA 24	-3	-22	38	3.72	< 0.001	
R Paracentral Lobule, BA 31	2	-21	44	3.7	< 0.001	
L Middle Temporal Gyrus, BA 20	**-53**	**-38**	**-6**	**3.75**	**< 0.001**	**168**
L Middle Temporal Gyrus, BA 22	-53	-43	5	3.21	0.001	

2B

Location	Talairach and Tournoux coordinates			peak	p value	cluster
	x	y	z	z-value	uncorr.	extension
L Medial Frontal Gyrus, BA 32	-5	7	45	4.19	< 0.001	133
L Medial Frontal Gyrus, BA 6	-7	3	51	3.56	< 0.001	
L Cingulate Gyrus, BA 24	-5	6	37	3.43	< 0.001	
R Cingulate Gyrus, BA 32	4	17	42	3.94	< 0.001	161
R Superior Frontal Gyrus, BA 6	4	5	52	3.89	< 0.001	
L Middle Temporal Gyrus, BA 20	-53	-38	-6	3.94	< 0.001	172

Previous literature reports of perturbed cerebral metabolism in LLD differ considerably in design; most of these investigations have concerned patients with major depressive disorder in contrast to the present subclinical depressed study group. Furthermore most of these studies used voxel-wise approaches, for instance Smith *et al.* reported increased FDG

Table 3. Significant (p < 0.05, bold) findings of VOI-based analysis of normalized [^{18}F]-fluorodeoxyglucose uptake in individual PET space for uncorrected (columns 2-6) and partial volume effect corrected (columns 8-12) data (column 1). [^{18}F]-fluorodeoxyglucose standard-uptake-value-ratio's (SUVR$_{VOI/CBL}$; mean ± SE) are reported for subclinical depressed (DEP; columns 2 + 8) and non-depressed subjects (NON-DEP; columns 3 + 9). F = F-statistics. p = p-value; ηp^2 = partial Eta-squared.

	Uncorrected					PVE-corrected				
	DEP (SUVR$_{VOI/CBL}$ mean ± SE)	NON-DEP (SUVR$_{VOI/CBL}$ mean ± SE)	F	ηp	ηp^2	DEP (SUVR$_{VOI/CBL}$ mean ± SE)	NON-DEP (SUVR$_{VOI/CBL}$ mean ± SE)	F	p	ηp^2
Frontal Lobe										
L mid frontal gyrus	1.14 ± 0.02	1.22 ± 0.02	6.47	**0.015**	0.14	1.55 ± 0.03	1.65 ± 0.03	5.24	**0.027**	0.11
R mid frontal gyrus	1.16 ± 0.02	1.22 ± 0.02	4.45	**0.041**	0.10	1.55 ± 0.03	1.62 ± 0.03	3.03	0.089	0.07
L precentral gyrus	1.06 ± 0.02	1.14 ± 0.02	8.98	**0.005**	0.18	1.76 ± 0.04	1.89 ± 0.04	4.82	**0.034**	0.11
R precentral gyrus	1.07 ± 0.02	1.14 ± 0.02	6.44	**0.015**	0.14	1.80 ± 0.03	1.88 ± 0.03	3.37	0.074	0.08
L inf frontal gyrus	1.11 ± 0.02	1.19 ± 0.02	8.71	**0.005**	0.18	1.47 ± 0.03	1.58 ± 0.03	7.90	**0.008**	0.16
R inf frontal gyrus	1.14 ± 0.02	1.19 ± 0.02	4.70	**0.036**	0.10	1.47 ± 0.03	1.54 ± 0.02	4.01	0.052	0.09
L sup frontal gyrus	1.06 ± 0.02	1.13 ± 0.02	7.31	**0.010**	0.15	1.52 ± 0.03	1.59 ± 0.02	3.83	0.057	0.09
R sup frontal gyrus	1.06 ± 0.02	1.12 ± 0.02	6.36	**0.016**	0.13	1.50 ± 0.03	1.57 ± 0.02	3.10	0.086	0.07
L orbitofrontal cortex - ant orbital gyrus	1.10 ± 0.02	1.16 ± 0.02	4.13	**0.049**	0.09	1.49 ± 0.03	1.53 ± 0.03	1.25	0.271	0.03
L orbitofrontal cortex - lat orbital gyrus	1.07 ± 0.02	1.13 ± 0.02	5.15	**0.029**	0.11	1.45 ± 0.03	1.54 ± 0.03	4.32	**0.044**	0.10
L orbitofrontal cortex - post orbital gyrus	1.03 ± 0.02	1.08 ± 0.02	4.70	**0.036**	0.10	1.25 ± 0.03	1.35 ± 0.02	6.52	**0.015**	0.14
L area subcallosa	0.81 ± 0.03	0.87 ± 0.02	4.31	**0.044**	0.10	0.81 ± 0.06	0.86 ± 0.05	0.34	0.560	0.01
Temporal Lobe										
L amygdala	0.77 ± 0.02	0.81 ± 0.02	2.03	0.162	0.05	0.78 ± 0.02	0.84 ± 0.02	4.99	**0.031**	0.11
L sup post temporal gyrus	1.05 ± 0.02	1.10 ± 0.01	4.43	**0.041**	0.10	1.41 ± 0.02	1.49 ± 0.02	7.98	**0.007**	0.16
L mid temporal gyrus	0.97 ± 0.02	1.01 ± 0.01	3.59	0.065	0.08	1.19 ± 0.02	1.24 ± 0.02	5.44	**0.025**	0.12
L post temporal lobe	1.01 ± 0.02	1.07 ± 0.01	9.94	**0.003**	0.20	1.15 ± 0.02	1.22 ± 0.01	7.40	**0.010**	0.15
Parietal Lobe										
L postcentral gyrus	1.02 ± 0.02	1.09 ± 0.02	8.06	**0.007**	0.16	1.70 ± 0.04	1.79 ± 0.04	2.34	0.134	0.05
R postcentral gyrus	1.04 ± 0.02	1.10 ± 0.02	4.69	**0.036**	0.10	1.74 ± 0.04	1.78 ± 0.04	0.69	0.410	0.02
L sup parietal gyrus	1.10 ± 0.02	1.21 ± 0.02	15.60	**0.000**	0.28	1.53 ± 0.03	1.62 ± 0.02	4.65	**0.037**	0.10
R sup parietal gyrus	1.11 ± 0.02	1.20 ± 0.02	14.60	**0.000**	0.26	1.55 ± 0.03	1.63 ± 0.03	4.70	**0.036**	0.10
L lat parietal lobe	1.04 ± 0.02	1.13 ± 0.02	14.28	**0.001**	0.26	1.37 ± 0.02	1.46 ± 0.02	6.44	**0.015**	0.14
R lat parietal lobe	1.06 ± 0.02	1.13 ± 0.02	8.00	**0.007**	0.16	1.37 ± 0.03	1.44 ± 0.02	3.46	0.070	0.08
Occipital Lobe										
L lingual gyrus	1.21 ± 0.02	1.28 ± 0.02	6.00	**0.019**	0.13	1.46 ± 0.04	1.53 ± 0.03	2.34	0.134	0.05
R lingual gyrus	1.22 ± 0.02	1.29 ± 0.02	4.87	**0.033**	0.11	1.50 ± 0.03	1.58 ± 0.03	3.02	0.090	0.07
L lat occipital gyrus	1.06 ± 0.02	1.14 ± 0.02	7.08	**0.011**	0.15	1.43 ± 0.04	1.52 ± 0.03	3.09	0.086	0.07
R lat occipital gyrus	1.07 ± 0.02	1.14 ± 0.02	6.73	**0.013**	0.14	1.45 ± 0.03	1.55 ± 0.03	4.42	**0.042**	0.10

	Uncorrected					PVE-corrected				
	DEP (SUVR$_{VOI/CBL}$ mean ± SE)	**NON-DEP** (SUVR$_{VOI/CBL}$ mean ± SE)	**F**	**p**	**np^2**	**DEP** (SUVR$_{VOI/CBL}$ mean ± SE)	**NON-DEP** (SUVR$_{VOI/CBL}$ mean ± SE)	**F**	**p**	**np^2**
L cuneus	1.20 ± 0.02	1.30 ± 0.02	10.13	**0.003**	0.20	1.55 ± 0.04	1.65 ± 0.03	4.41	**0.042**	0.10
R cuneus	1.23 ± 0.02	1.32 ± 0.02	8.49	**0.006**	0.17	1.60 ± 0.04	1.68 ± 0.03	2.25	0.141	0.05
Insula and Cingulate Gyri										
L insula	0.99 ± 0.02	1.05 ± 0.01	7.30	**0.010**	0.15	0.99 ± 0.02	1.07 ± 0.02	8.26	**0.006**	0.17
L ant cingulate gyrus	0.99 ± 0.02	1.07 ± 0.02	9.04	**0.005**	0.18	1.14 ± 0.03	1.20 ± 0.02	2.64	0.112	0.06
R ant cingulate gyrus	0.99 ± 0.02	1.07 ± 0.02	9.28	**0.004**	0.19	1.15 ± 0.03	1.20 ± 0.02	2.03	0.162	0.05
L post cingulate gyrus	1.19 ± 0.02	1.31 ± 0.02	19.00	**0.000**	0.32	1.38 ± 0.03	1.45 ± 0.02	3.81	0.058	0.09
R post cingulate gyrus	1.19 ± 0.02	1.30 ± 0.02	14.57	**0.000**	0.26	1.37 ± 0.03	1.44 ± 0.02	3.80	0.058	0.09
Central structures										
L thalamus	0.91 ± 0.02	1.00 ± 0.02	10.85	**0.002**	0.21	0.93 ± 0.02	1.03 ± 0.02	9.59	**0.004**	0.19
R thalamus	0.93 ± 0.02	1.00 ± 0.02	7.48	**0.009**	0.15	0.96 ± 0.02	1.05 ± 0.02	6.83	**0.012**	0.14
L substantia nigra	0.83 ± 0.02	0.89 ± 0.02	4.37	**0.043**	0.10	1.32 ± 0.06	1.44 ± 0.06	1.95	0.170	0.05
R substantia nigra	0.80 ± 0.02	0.85 ± 0.02	4.20	**0.047**	0.09	1.23 ± 0.06	1.35 ± 0.05	2.19	0.146	0.05
R nucleus accumbens	0.97 ± 0.02	1.03 ± 0.02	5.01	**0.031**	0.11	1.43 ± 0.06	1.56 ± 0.05	3.54	0.067	0.08
L putamen	1.24 ± 0.02	1.30 ± 0.02	6.08	**0.018**	0.13	1.34 ± 0.03	1.43 ± 0.02	6.00	**0.019**	0.13
L pallidum	1.02 ± 0.02	1.08 ± 0.01	7.26	**0.010**	0.15	1.23 ± 0.03	1.29 ± 0.02	2.80	0.102	0.06
Brainstem	0.73 ± 0.01	0.77 ± 0.01	5.97	**0.019**	0.13	0.68 ± 0.01	0.71 ± 0.01	3.87	0.056	0.09

uptake in the ACC of untreated, aged subjects with depression contrasted with healthy, and also reported a correlation of this metabolic increase with symptom severity and cerebral atrophy. Treatment with SSRIs or total sleep deprivation decreased the anterior cortical and limbic metabolism, but increased posterior cortical, putaminal and cerebellar metabolism relative to pre-treatment baseline (7-10, 44). On the other hand, LLD patients showed hypermetabolism in ACC and insula and a hypometabolism in posterior parts upon treatment with SSRI after 2 years in a longitudinal analysis [11].

In depressed patients with MCI or AD, hypometabolism was previously observed in the right superior frontal gyrus (Brodman Area, BA6) [14, 15], as we likewise see in the present CN elderly patients positive for DEP symptoms. Two previous FDG-PET investigations of AD patients assessed DEP scores using the NPI (long form); in one such study of early AD subjects, clinically significant depression was associated with hypometabolism in left superior and inferior frontal cortices [13], whereas in the other study, there was a significant correlation between depression scores and hypometabolism in bilateral superior frontal and left anterior cingulate cortices [12]. Furthermore a recent FDG-PET investigation revealed a link between increased fasting serum glucose levels and decreased cerebral glucose metabolism, which was even more pronounced in LLD when compared to elderly controls [45]. Thus, there is considerable precedent for the present finding that even subclinical depression in non-demented elderly patients may be associated with relative hypometabolism in frontal structures.

4.2. Atrophy Correction

Real findings of hypometabolism can be accentuated by cerebral atrophy, as certainly occurs in the conversion to MCI and dementia. A recent MRI study in which depression was assessed by the NPI-Q, showed greater frontal, parietal and temporal WM atrophy during 24 month follow-up in depressed MCI patients contrasted with non-depressed MCI [6], which would predict some bias in FDG measurements. Reduced volume was also found in frontal cortex, ACC, hippocampus and amygdala in depressed CN subjects [20-22]. In our study, only 3 of 75 GM regions showed statistically significant volume reductions in the DEP group. Nonetheless, applying the PVEC propagated to large changes in the pattern of hypometabolism, with losses of detectable differences in some regions (frontal, occipital and cingulate cortices) and additional findings of significant differences in other regions (amygdala, insula, temporal cortex). Hence, we find that MRI- and VOI-based PVEC is essential for distinguishing real and atrophy-related change in cerebral metabolism in patients with depressive symptoms. Discrepancies in earlier investigations could at least partly by explainable due to lack of atrophy correction.

4.3. VOI-based Approach

Nearly all investigations targeting cerebral metabolism of depressed subjects have used SPM for FDG-PET analysis.

While convenient, the SPM method suffers from disadvantages arising from spatial normalization through nonlinear alignments weighted to surface features of the FDG-PET, which result in lower accuracy of deep brain structures. We circumvented this problem by carrying out an additional MRI-based SUVR$_{VOI/CBL}$ analysis in individual PET space. Visual inspection after automatic VOI configuration showed good fitting accuracy, and led to good agreement with SPM findings on the cortical surface, while revealing additional significant group differences in non-surface regions such as left insula, left amygdala, and deep nuclei. The complete pattern of FDG-PET changes seems to match mood disorder neurocircuitry, which serves to validate our VOI-based approach. Furthermore, standardized quantitative assessments are facilitated by VOI-based approaches and could make FDG-PET studies more comparable when contrasted against similar investigations.

4.4. Limitations

We excluded patients with any neuropsychiatric symptoms other than depression, resulting at a low sample size precluded longitudinal follow-up imaging, additional amyloid imaging, or follow-up of conversion rates. However, this seemed of importance as for instance apathy was found to influence brain metabolism as well [46]. Further studies could reveal if focally decreased metabolism predicts higher conversion rates in CN LLD subjects, and if this occurs in association with amyloidosis. The ADNI originally was not designed to address a particular hypothesis with regard to depressive symptoms in elderly CN subjects. Beside this potential bias it notwithstanding allowed us to test well-matched cohorts with the above mentioned low confounding by other neuropsychiatric symptoms. 13 of 21 DEP subjects received chronic psychotropic medication, including S(N)SRI (N = 9); previous work shows that chronic SSRI can evoke widespread metabolic decreases in some of the regions noted in the present group and also metabolic increases [7]. Indeed, subdivision of the DEP group revealed a trend towards lower metabolism in the medicated subjects, such that confounding effects of medication cannot be excluded. Finally, the assessment of depressive symptoms with NPI-Q is not detailed, when for example compared to gold standard structured clinical interview assessment in the field of depression. Although the NPI-Q it is sufficient to predict the risk factor (OR 2.9) for conversion from CN to MCI, and is in this respect more sensitive than GDS (OR 1.9) [4].

CONCLUSION

CN elderly subjects with depressive symptoms revealed decreased FDG metabolism in mood-related fronto-temporal brain regions, which may be relevant to their reportedly increased risk for conversion from CN to MCI. The small sample size was contingent upon strict inclusion criteria, but nevertheless allowed us to examine a collective largely free of confounding covariates. Although few regions in DEP patients had significant atrophy, PVEC had considerable impact on locating metabolic differences between DEP and NON-DEP subjects. This finding emphasizes the need of atrophy correction in brain PET studies of aged subjects. MRI-based VOI analysis in native PET space proved superior for detecting subcortical differences when compared to SPM analysis, and will contribute to more precision in PET analyses of neurocircuitry in deeper brain areas.

ABBREVIATIONS

ACC	=	Anterior cingulate cortex
AD	=	Alzheimer's disease
ADNI	=	Alzheimer's Disease Neuroimaging Initiative
CN	=	cognitively normal
CSF	=	cerebro-spinal fluid
DEP	=	subjects with depressive symptoms
FDA	=	Food and Drug Administration
FDG-PET	=	[^{18}F]-fluorodesoxyglucose positron emission tomography
GDS	=	geriatric depression scale
GM	=	grey matter
LLD	=	Late life depression
MANCOVA	=	multivariate analysis of covariance
MCI	=	mild cognitive impairment
MGM	=	MRI based PVEC by Müller Gärtner method
MMSE	=	mini mental state examination
MNI	=	Montreal Neurological Institute
MRI	=	magnetic resonance imaging
NIA	=	National Institute on Aging
NIBIB	=	National Institute of Biomedical Imaging and Bioengineering
NON-DEP	=	subjects without depressive symptoms
NPI-Q	=	Neuropsychiatric Inventory Questionnaire
PCC	=	posterior cingulate cortex
PVEC	=	partial volume effect correction
S(N)SRI	=	serotonin-(noradrenaline)-reuptake-inhibitors
SPM	=	statistical-parametric-mapping
SUVR	=	standard-uptake-value-ratios
T1w	=	T1-weighted
VOI	=	volume-of-interest
WM	=	white matter

CONFLICT OF INTEREST

ACKNOWLEDGEMENTS

REFERENCES

[1] Ziegler-Graham K, Brookmeyer R, Johnson E, Arrighi HM. Worldwide variation in the doubling time of Alzheimer's disease incidence rates. Alzheimers Dement 4(5): 316-23 (2008).

[2] Ownby RL, Crocco E, Acevedo A, John V, Loewenstein D. Depression and risk for Alzheimer disease: systematic review, meta-analysis, and metaregression analysis. Arch Gen Psychiatry 63(5): 530-8 (2006).

[3] Olin JT, Katz IR, Meyers BS, Schneider LS, Lebowitz BD. Provisional diagnostic criteria for depression of Alzheimer disease: rationale and background. Am J Geriatr Psychiatry 10(2): 129-41 (2002).

[4] Steenland K, Karnes C, Seals R, Carnevale C, Hermida A, Levey A. Late-life depression as a risk factor for mild cognitive impairment or Alzheimer's disease in 30 US Alzheimer's disease centers. J Alzheimers Dis 31(2): 265-75 (2012).

[5] Mayberg HS, Lozano AM, Voon V, McNeely HE, Seminowicz D, Hamani C, et al. Deep brain stimulation for treatment-resistant depression. Neuron 45(5): 651-60 (2005).

[6] Lee GJ, Lu PH, Hua X, Lee S, Wu S, Nguyen K, et al. Depressive symptoms in mild cognitive impairment predict greater atrophy in Alzheimer's disease-related regions. Biol Psychiatry 71(9): 814-21 (2012).

[7] Smith GS, Kramer E, Hermann CR, Goldberg S, Ma Y, Dhawan V, et al. Acute and chronic effects of citalopram on cerebral glucose metabolism in geriatric depression. Am J Geriatr Psychiatry 10(6): 715-23 (2002).

[8] Smith GS, Reynolds CF, 3rd, Houck PR, Dew MA, Ma Y, Mulsant BH, et al. Glucose metabolic response to total sleep deprivation, recovery sleep, and acute antidepressant treatment as functional neuroanatomic correlates of treatment outcome in geriatric depression. Am J Geriatr Psychiatry 10(5): 561-7 (2002).

[9] Smith GS, Kramer E, Hermann C, Ma Y, Dhawan V, Chaly T, et al. Serotonin modulation of cerebral glucose metabolism in depressed older adults. Biol Psychiatry 66(3): 259-66 (2009).

[10] Smith GS, Kramer E, Ma Y, Kingsley P, Dhawan V, Chaly T, et al. The functional neuroanatomy of geriatric depression. Intern J Geriatr Psychiatry 24(8): 798-808 (2009).

[11] Marano CM, Workman CI, Kramer E, Hermann CR, Ma Y, Dhawan V, et al. Longitudinal studies of cerebral glucose metabolism in late-life depression and normal aging. Intern J Geriatr Psychiatry 28(4): 417-23 (2013).

[12] Hirono N, Mori E, Ishii K, Ikejiri Y, Imamura T, Shimomura T, et al. Frontal lobe hypometabolism and depression in Alzheimer's disease. Neurology 50(2): 380-3 (1998).

[13] Holthoff VA, Beuthien-Baumann B, Kalbe E, Ludecke S, Lenz O, Zundorf G, et al. Regional cerebral metabolism in early Alzheimer's disease with clinically significant apathy or depression. Biol Psychiatry 57(4): 412-21 (2005).

[14] Lee DY, Choo IH, Jhoo JH, Kim KW, Youn JC, Lee DS, et al. Frontal dysfunction underlies depressive syndrome in Alzheimer disease: a FDG-PET study. Am J Geriatr Psychiatry 14(7): 625-8 (2006).

[15] Lee HS, Choo IH, Lee DY, Kim JW, Seo EH, Kim SG, et al. Frontal Dysfunction Underlies Depression in Mild Cognitive Impairment: A FDG-PET Study. Psychiatry Investig 7(3): 208-14 (2010).

[16] Price JL, Drevets WC. Neurocircuitry of mood disorders. Neuropsychopharmacology 35(1): 192-216 (2010).

[17] Amaral DG, Insausti R. Retrograde transport of D-[3H]-aspartate injected into the monkey amygdaloid complex. Exp Brain Res Exp Hirnforsch Exp Cereb 88(2): 375-88 (1992).

[18] Russchen FT, Bakst I, Amaral DG, Price JL. The amygdalostriatal projections in the monkey. An anterograde tracing study. Brain Res 329(1-2): 241-57 (1985).

[19] Russchen FT, Amaral DG, Price JL. The afferent input to the magnocellular division of the mediodorsal thalamic nucleus in the monkey, Macaca fascicularis. J Comparat Neurol 256(2): 175-210 (1987).

[20] Ballmaier M, Sowell ER, Thompson PM, Kumar A, Narr KL, Lavretsky H, et al. Mapping brain size and cortical gray matter changes in elderly depression. Biol Psychiatry 55(4): 382-9 (2004).

[21] Campbell S, Marriott M, Nahmias C, MacQueen GM. Lower hippocampal volume in patients suffering from depression: a meta-analysis. Am J Psychiatry 161(4): 598-607 (2004).

[22] Egger K, Schocke M, Weiss E, Auffinger S, Esterhammer R, Goebel G, et al. Pattern of brain atrophy in elderly patients with depression revealed by voxel-based morphometry. Psychiatry Res 164(3): 237-44 (2008).

[23] Butters MA, Klunk WE, Mathis CA, Price JC, Ziolko SK, Hoge JA, et al. Imaging Alzheimer pathology in late-life depression with PET and Pittsburgh Compound-B. Alzheimer Dis Assoc Disord 22(3): 261-8 (2008).

[24] Wu KY, Hsiao IT, Chen CS, Chen CH, Hsieh CJ, Wai YY, et al. Increased brain amyloid deposition in patients with a lifetime history of major depression: evidenced on F-florbetapir (AV-45/Amyvid) positron emission tomography. Eur J Nucl Med Mol Imaging 41(4): 714-22 (2014).

[25] Madsen K, Hasselbalch BJ, Frederiksen KS, Haahr ME, Gade A, Law I, et al. Lack of association between prior depressive episodes and cerebral [11C]PiB binding. Neurobiol Aging 33(10): 2334-42 (2012).

[26] Erlandsson K, Buvat I, Pretorius PH, Thomas BA, Hutton BF. A review of partial volume correction techniques for emission tomography and their applications in neurology, cardiology and oncology. Phys Med Biol 57(21): R119-59 (2012).

[27] Kaufer DI, Cummings JL, Ketchel P, Smith V, MacMillan A, Shelley T, et al. Validation of the NPI-Q, a brief clinical form of the Neuropsychiatric Inventory. J Neuropsychiatr Clin Neurosci 12(2): 233-9 (2000).

[28] Brendel M, Pogarell O, Xiong G, Delker A, Bartenstein P, Rominger A, et al. Depressive symptoms accelerate cognitive decline in amyloid-positive MCI patients. Eur J Nucl Med Mol Imaging 42(5): 716-24 (2015).

[29] Koppel J, Sunday S, Goldberg TE, Davies P, Christen E, Greenwald BS, et al. Psychosis in Alzheimer's disease is associated with frontal metabolic impairment and accelerated decline in working memory: findings from the Alzheimer's disease neuroimaging initiative. Am J Geriatr Psychiatry 22(7): 698-707 (2014).

[30]   Burke WJ, Roccaforte WH, Wengel SP. The short form of the Geriatric Depression Scale: a comparison with the 30-item form. J Geriatr Psychiatry Neurol 4(3): 173-8 (1991).

[31]   Sanabria-Diaz G, Martinez-Montes E, Melie-Garcia L, Alzheimer's Disease Neuroimaging I. Glucose metabolism during resting state reveals abnormal brain networks organization in the Alzheimer's disease and mild cognitive impairment. PLoS One 8(7): e68860 (2013).

[32]   Jack CR, Jr., Bernstein MA, Fox NC, Thompson P, Alexander G, Harvey D, et al. The Alzheimer's Disease Neuroimaging Initiative (ADNI): MRI methods. J Mag Reson Imaging 27(4): 685-91 (2008).

[33]   Jovicich J, Czanner S, Greve D, Haley E, van der Kouwe A, Gollub R, et al. Reliability in multi-site structural MRI studies: effects of gradient non-linearity correction on phantom and human data. NeuroImage 30(2): 436-43 (2006).

[34]   Sled JG, Zijdenbos AP, Evans AC. A nonparametric method for automatic correction of intensity nonuniformity in MRI data. IEEE Trans Med Imaging 17(1): 87-97 (1998).

[35]   Ortiz A, Gorriz JM, Ramirez J, Martinez-Murcia FJ, Alzheimer's Disease Neuroimaging I. Automatic ROI selection in structural brain MRI using SOM 3D projection. PLoS One 9(4): e93851 (2014).

[36]   Jack CR, Jr., Bernstein MA, Fox NC, Thompson P, Alexander G, Harvey D, et al. The Alzheimer's Disease Neuroimaging Initiative (ADNI): MRI methods. J Magn Reson Imaging 27(4): 685-91 (2008).

[37]   Dukart J, Mueller K, Horstmann A, Vogt B, Frisch S, Barthel H, et al. Differential effects of global and cerebellar normalization on detection and differentiation of dementia in FDG-PET studies. NeuroImage 49(2):1490-5 (2010).

[38]   Mielke R, Pietrzyk U, Jacobs A, Fink GR, Ichimiya A, Kessler J, et al. HMPAO SPET and FDG PET in Alzheimer's disease and vascular dementia: comparison of perfusion and metabolic pattern. Eur J Nuc Med 21(10): 1052-60 (1994).

[39]   Hammers A, Allom R, Koepp MJ, Free SL, Myers R, Lemieux L, et al. Three-dimensional maximum probability atlas of the human brain, with particular reference to the temporal lobe. Hum Brain Mapp 19(4): 224-47 (2003).

[40]   Ashburner J, Friston KJ. Unified segmentation. NeuroImage 26(3): 839-51 (2005).

[41]   Muller-Gartner HW, Links JM, Prince JL, Bryan RN, McVeigh E, Leal JP, et al. Measurement of radiotracer concentration in brain gray matter using positron emission tomography: MRI-based correction for partial volume effects. J Cereb Blood Flow Metab 12(4): 571-83 (1992).

[42]   Rousset OG, Ma Y, Evans AC. Correction for partial volume effects in PET: principle and validation. J Nucl Med 39(5): 904-11 (1998).

[43]   Rousset OG, Collins DL, Rahmim A, Wong DF. Design and implementation of an automated partial volume correction in PET: application to dopamine receptor quantification in the normal human striatum. J Nucl Med 49(7): 1097-106 (2008).

[44]   Diaconescu AO, Kramer E, Hermann C, Ma Y, Dhawan V, Chaly T, et al. Distinct functional networks associated with improvement of affective symptoms and cognitive function during citalopram treatment in geriatric depression. Hum Brain Mapp 32(10):1677-91 (2011).

[45]   Marano CM, Workman CI, Lyman CH, Kramer E, Hermann CR, Ma Y, et al. The relationship between fasting serum glucose and cerebral glucose metabolism in late-life depression and normal aging. Psychiatr Res 222(1-2): 84-90 (2014).

[46]   Delrieu J, Desmidt T, Camus V, Sourdet S, Boutoleau-Bretonniere C, Mullin E, et al. Apathy as a feature of prodromal Alzheimer's disease: an FDG-PET ADNI study. Intern J Geriatr Psychiatry 30(5): 470-7 (2015).